Published in final edited form as:
Science. 2017 May 12; 356(6338): 617–624. doi:10.1126/science.aah6152.

Reticulon3-dependent ER-PM contact sites control EGFR non-clathrin endocytosis

Giusi Caldieri[1,*], **Elisa Barbieri**[1,*], **Gilda Nappo**[1,*], **Andrea Raimondi**[4,*], **Massimo Bonora**[6], **Alexia Conte**[1], **Lisette G.G.C. Verhoef**[1,a], **Stefano Confalonieri**[1], **Maria Grazia Malabarba**[1,2], **Fabrizio Bianchi**[3,b], **Alessandro Cuomo**[3], **Tiziana Bonaldi**[3], **Emanuele Martini**[1], **Davide Mazza**[4], **Paolo Pinton**[6], **Carlo Tacchetti**[4,5], **Simona Polo**[1,2], **Pier Paolo Di Fiore**[1,2,3,#], and **Sara Sigismund**[1,#]

[1]IFOM, Fondazione Istituto FIRC di Oncologia Molecolare, Via Adamello 16, 20139, Milan, Italy

[2]Dipartimento di Oncologia ed Emato-Oncologia (DiPO) - Università degli Studi di Milano, Via Festa del Perdono, 7, 20122, Milan, Italy

[3]Istituto Europeo di Oncologia, Via Ripamonti 435, 20141, Milan, Italy

[4]Centro Imaging Sperimentale, IRCCS Istituto Scientifico San Raffaele, Via Olgettina 52, 20132 Milan, Italy

[5]Dipartimento di Medicina Sperimentale, Università degli Studi di Genova, Genoa, Italy

[6]Section of Pathology, Oncology and Experimental Biology and Laboratory for Technologies of Advanced Therapies Center, Department of Morphology, Surgery and Experimental Medicine, University of Ferrara, Ferrara, Italy

Abstract

The integration of endocytic routes is critical to regulate receptor signaling. A non-clathrin endocytic pathway (NCE) of the epidermal growth factor receptor (EGFR) is activated at high ligand concentrations and targets receptors to degradation, attenuating signaling. Here we performed an unbiased molecular characterization of EGFR-NCE. We identified NCE-specific regulators, including the endoplasmic reticulum (ER)-resident protein reticulon-3 (RTN3), and a specific cargo, CD147. RTN3 was critical for EGFR/CD147-NCE, promoting the creation of plasma membrane (PM)–ER contact sites that were required for the formation/maturation of NCE invaginations. Ca^{2+} release at these sites, triggered by IP3-dependent activation of ER Ca^{2+} channels, was needed for the completion of EGFR internalization. Thus, we identified a mechanism of EGFR endocytosis that relies on ER-PM contact sites and local Ca^{2+} signaling.

Correspondence to: SS, sara.sigismund@ifom.eu, or to PPDF, pierpaolo.difiore@ifom.eu.
[a]Current address: Center for Genomic Science of IIT@SEMM, Istituto Italiano di Tecnologia, Via Adamello 16, 20139 Milan, Italy.
[b]Current address:!SBReMIT - Institute for Stem-cell Biology, Regenerative Medicine and Innovative Therapies, IRCCS - Casa Sollievo della Sofferenza,Viale Cappuccini s.n.c, 71013 San Giovanni Rotondo, Foggia, Italy.
[*]These authors contributed equally;
[#]SS and PPDF contributed equally

Europe PMC Funders Author Manuscripts

Introduction

While clathrin-mediated endocytosis (CME) represents the best characterized internalization route into cells (1), several non-clathrin endocytosis (NCE) pathways exist that specify diversified functions and/or fates of individual cargoes (2).

Ligand-induced internalization of epidermal growth factor receptor (EGFR) occurs through both CME and NCE, depending on growth conditions and cellular context (3–6). At low EGF dose (1 ng/ml), EGFRs are primarily internalized by CME and recycled back to the plasma membrane (PM), with ~30% receptors targeted to degradation (7). At high, physiological, EGF concentrations (20-100 ng/ml), NCE gets activated in parallel to CME. EGFRs entering via NCE (~40%) are predominantly trafficked to the lysosome for degradation, leading to signal extinction (7, 8). Thus, NCE might serve as a negative regulator of EGFR signaling in response to excessive stimuli.

EGFR-NCE is apparently distinct from other endocytic pathways (Table S1). It is cholesterol- and dynamin-dependent, but caveolin-independent, and requires EGFR ubiquitination and proteins harboring Ub-binding domains (4, 8). However, a detailed understanding of its molecular workings is lacking. Such knowledge would help in our understanding of how the cell has developed different mechanisms of endocytosis to control the balance between positive and negative regulation of receptor signaling. Moreover, given the established role of EGFR in oncogenesis (9), it might provide insights into possible mechanisms of tumorigenesis, because NCE displays the characteristics of a tumor suppressor mechanism. Here, we provide a comprehensive molecular portrait of the pathway and details of the mechanism underlying NCE.

Results

Molecular characterization of EGFR-NCE

To identify proteins involved in EGFR-NCE, we performed a SILAC analysis of purified EGFR-containing NCE vesicles (10). Vesicles were purified under conditions of inducible clathrin knockdown (KD) (Fig. 1A and S1). Although this approach only yielded a partially-purified vesicle fraction, the high discriminatory power of SILAC allowed us to identify EGFR-NCE candidates by comparing vesicles from EGF-stimulated clathrin KD cells *vs.* unstimulated cells, representing the ‘background’ (Fig. 1B).

Three experiments yielded overlapping proteomes (~60%, Fig. 1C and File S1, spreadsheet 1), with a bimodal distribution of SILAC ratios (Fig. 1D and File S1, spreadsheet 2). The major peak, centered on a H/L Ratio of ~1 (Log2 Ratio ~0), represents proteins equally present in the two samples (presumably contaminants); the minor peak, centered on H/L Ratio ~2.3 (Log2 Ratio ~1.2), should be enriched in EGFR-NCE components. To select candidates for validation, we applied high confidence filters: proteins present in the top 20%, ranked by H/L ratios, in 3 out of 3 replicates and robustly quantified (ratio count, RC >2). This selection process yielded 151 proteins (Fig. 1D and File S1, spreadsheet 3), of which 101 were tested in validation experiments (File S1, spreadsheet 3-4).

Validation of SILAC candidates

To validate candidates, we silenced their expression in inducible clathrin KD cells and analyzed EGFR internalization following stimulation with high dose EGF (Fig. S2A, 1). We scored an effect on EGFR-NCE for 43 candidates (File S2, spreadsheets 1-2). These candidates were then screened for their effects on: i) EGFR-NCE upon transient clathrin KD (to obtain replicates and exclude clonal effects); ii) EGFR-CME at low EGF doses; iii) transferrin receptor (TfR)-CME; iv) surface EGFR number, since this might affect the internalization constants (Fig. S2A, 2 and File S2, spreadsheets 3-9). After deconvolution analysis (Fig. S2A, 3), we derived a list of 9 EGFR-NCE regulators, which included signal-transduction, RNA-binding and endoplasmic reticulum (ER)/mitochondrial proteins (Fig. 2A), not previously implicated in internalization pathways (Table S1, Fig. S2D-G).

RTN3 is a critical regulator of EGFR-NCE

Of the 9 candidate EGFR-NCE regulators, the ER tubulation factor reticulon-3 (RTN3) (11) showed one of the strongest phenotypes (Fig. 2A). KD of RTN3 resulted in ~50% reduction in EGF internalization at high dose (Fig. 2B), compatible with the proportion of EGFRs entering via NCE (4). The double RTN3/clathrin KD reduced EGF internalization almost to the levels observed under dynamin KD (Fig. 2B,C and S2B), demonstrating its requirement for EGFR-NCE. Conversely, RTN3 KD had a minor impact on EGFR internalization at low EGF doses and no effect on Tf internalization (Fig. 2B,D).

Another ER-shaping factor, REEP5, also had a significant effect on NCE (Fig. 2A). RTN3 and REEP5 form a complex with another reticulon, RTN4, and this complex is implicated in cortical ER tubulation (11, 12). However, RTN4 KD did not affect EGFR internalization (Fig. 2B and S2C), arguing for a specific function of RTN3 and REEP5 in NCE.

NCE preferentially targets EGFRs to degradation (7). Accordingly, RTN3 KD significantly delayed EGFR and EGF degradation (Fig. 2E,F), reduced EGFR trafficking towards multivesicular bodies (MVBs, Fig. S3A), and increased EGF-induced signaling (Fig. 2G).

RTN3 is required for the maturation of NCE intermediates at the PM

We characterized EGFR-NCE by electron microscopy (EM). In control cells, gold-labeled EGFR was detectable in clathrin-coated pits (CCPs) and in tubular invaginations (TI, diameter ≈80 nm, Fig. 3A,B and S3B). TIs persisted in clathrin KD cells (Fig. 3A,B), suggesting that they might represent the structures mediating EGFR-NCE. TIs are morphologically reminiscent of CLICs (clathrin-independent carriers) (13, 14), although the two pathways show distinct functional requirements (Table S1) (15).

In RTN3 KD cells, TIs were significantly reduced in number (Fig. 3A,B), while no effect was observed on CCPs (Fig. 3B), arguing that TIs are NCE intermediates whose formation/maturation is RTN3-dependent. Importantly, dynamin KD did not reduce TI number (Fig. 3B); rather, it increased the ratio of long (>300 nm) *vs.* short TIs (~150-300 nm, Fig. 3C). A similar phenotype was observed for CCPs, with a shift towards longer CCPs (>200 nm, Fig. 3C), as previously reported (16). These data argue that dynamin is involved in the fission of TIs (and CCPs), while RTN3 could act upstream, at the level of TI maturation. Indeed, the

RTN3 KD phenotype appeared epistatic to the dynamin one, because the double KD RTN3/dynamin closely resembled the single RTN3 KD phenotype (Fig. 3B).

We then followed gold-EGFR internalization by discriminating PM-connected *vs.* internalized structures with ruthenium red (RuR, Fig. S3C,D). In control cells, EGFR present in RuR-positive structures (CCPs and TIs) decreased over time, with a parallel increase of internalized receptors (Fig. 3D,E and S3D). In clathrin KD and RTN3 KD cells, gold-EGFR in intracellular structures significantly decreased (~50%), accompanied by an increase in RuR-positive structures (Fig. 3D,E and S3D), consistent with the inhibition of CME and NCE, respectively. In double clathrin/RTN3 KD cells, internalization was almost completely blocked (>80%), in agreement with ^{125}I-EGF internalization assays (Fig. 3F).

RTN3 localizes in close proximity to active EGFR

By immunofluorescence (IF), we confirmed that RTN3 is an ER-resident protein (Fig. S3E,F,G), located in the peripheral ER and colocalized with cortical ER markers involved in ER-PM contact sites, namely E-Syt1 and STIM1 [Fig. S3F and (17, 18)]. This result was verified by immuno-EM, which showed that RTN3 was exclusively associated with ER, and no PM signals, above background, could be evidenced (Fig. S3H).

By proximity ligation assays, RTN3 and activated EGFR were found in close proximity (within ~30 nm) upon EGF stimulation (Fig. S4A). To better define the RTN3 and EGFR association, we employed super-resolution microscopy and Förster resonance energy transfer (FRET). With the first approach, we observed, upon high EGF, increased co-clustering of EGFR and RTN3 (C_0) and an increase of cluster size (R_C) at the cell periphery *vs.* cells stimulated with low EGF dose or unstimulated (Fig. 4A). By FRET, a higher signal between RTN3 and EGFR was registered with high EGF dose compared with basal conditions (Fig. 4B). The signal was specific, because no signal was detectable for the pair TfR/RTN3 (Fig. S4B). The EGFR/RTN3 FRET signal is compatible with the scenario that peripheral ER comes into close proximity with active EGFR upon EGF stimulation. Indeed, other cortical ER proteins (RTN4, STIM1 and E-Syt1) gave a positive FRET signal within 5 minutes of EGF stimulation (Fig. 4B and S4C), while proteins not enriched in peripheral ER did not (Fig. 4B and S4C). When we restricted FRET analysis to the PM regions where EGFR is active (by applying a PM EGF-based mask, excluding endosomes) and followed the FRET signal kinetically in the initial phases of EGF stimulation (first 3 minutes), RTN3 was the sole marker that gave a significant FRET signal (Fig. 4C). In agreement, the KD of E-Syt and STIM proteins - as in the case of RTN4 - did not affect EGFR endocytosis (Fig. S4D and 2B).

RTN3 is required for ER-PM contact sites where EGFR-NCE occurs

The above results are compatible with the formation of RTN3-dependent EGF-induced contact sites between peripheral ER and NCE-TIs. We transfected cells with horseradish peroxidase (HRP)-KDEL peptide sequence (17, 19), to visualize the ER, and detected areas of ER-PM proximity, in regions that either contained or did not contain the EGFR (Fig. S5A). Initially, we explored the effect of RTN3 KD on general ER morphology, in parallel to RTN4 KD, which was previously shown to affect ER architecture by skewing ER peripheral

tubules towards cisternae (20). We confirmed the RTN4 KD phenotype in our cell system by 3D ER reconstruction, as evidenced by an increase in long ER profiles (>1000 nm) with concomitant decrease in shorter profiles (Fig. S5B). Conversely, in RTN3 KD cells, we did not observe major rearrangements in the distribution of ER profiles, confirming previously reported results obtained in RTN3 KO mouse embryonic fibroblasts (Fig. S5B) (21).

However, automated ER segmentation analysis on high-resolution images revealed that both RTN3 and RTN4 KD reduced the number of small tubular ER profiles, while only RTN4 KD increased large ER sheets (Fig. S5C). EGF stimulation caused an increase in tubular ER profiles within 20 nm of the PM, consistent with the formation of EGF-induced ER-PM contact sites. Although RTN3 and RTN4 KD had a similar impact on the tubulation of peripheral bulk ER (Fig. S5C), only RTN3 KD reduced the number of EGF-induced ER-PM contact sites (Fig. 4D).

Finally, we investigated the existence of specific RTN3-dependent contacts between ER and EGFR-NCE structures by performing serial sections and quantification of contacts between the ER (HRP-KDEL) and gold-EGFR-positive PM invaginations (NCE-TIs or CCPs). Serial sectioning allowed us to detect contact sites even when gold-labeled EGFR and ER were not visible in the same section (Fig. S5D and 4E). We considered as "contacts" those instances in which ER proximity (≤20 nm) to EGFR-gold-positive PM invaginations was present in at least one out of three sections (Fig. 4E). About 20% of the EGFR-containing PM-TIs were in contact with tubular ER, while there were no contacts between ER and CCPs. In RTN3 KD cells, the remaining TIs were not in contact with ER (Fig. 4E and S5D for distance-dependent analysis). Serial sectioning is prone to underestimate the phenomenon, bacause we inevitably lose some of the contacts between two consecutive sections (thickness of ~60 nm). Indeed, by performing tomograms (Z-axis resolution of ~3-6 nm) of 11 randomly selected CD147-positive TIs, we found that 8 out of the 11 TIs were in contact with an ER tubule (~70%, see Fig. S6 for extracts from 4 representative tomograms, and Movie S1).

CD147, a cargo internalizing through NCE

In the initial candidate list, there were many PM-resident proteins whose ablation did not alter EGFR-NCE. These proteins might represent cargoes of this pathway. As proof of principle of this concept, we focused on cluster of differentiation 147 (CD147)/Basigin (BSG).

CD147 colocalized with internalized EGF in clathrin KD cells (Fig. S7A), suggesting that it co-traffics with the EGFR through NCE. Thus, we followed CD147 endocytosis with an antibody that recognizes its extracellular domain without interfering with endocytosis (22). Upon EGF stimulation, CD147 was internalized and colocalized with EGF via a clathrin-independent process that was sensitive to RTN3 KD (Fig. 5A, B and Fig. S7B for controls). Importantly, CD147/EGFR internalization in RTN3 KD cells was restored by the reintroduction of RTN3A, which is the most expressed RTN3 isoform in HeLa cells (Fig. 5C and S8A-C).

Thus, upon EGF stimulation, CD147 enters the cell almost exclusively through NCE and can be used as a specific marker of this pathway. We exploited CD147 internalization as an

independent tool for the validation of the functional role of candidate NCE regulators. Silencing of the 9 regulators affected CD147 internalization upon EGF stimulation, corroborating their role in NCE and providing a cross-validation of both functional regulators and cargo (Fig. S9A).

We then used CD147 for EM analysis. By double PM (RuR)-CD147 (immunogold) staining, we found that after 5 min of EGF stimulation, CD147 was either at the PM or in TIs indistinguishable from those observed for the EGFR-NCE (Fig. 5D and S9B), but not in CCPs. RTN3 KD reduced the formation of CD147-positive TIs (Fig. 5D), arguing that TIs are indeed endocytic intermediates of CD147. Quantification of gold particles in PM-connected *vs.* internalized structures revealed that ~75% of CD147 was at the PM or in PM-connected TIs, with ~25% of gold particles internalized at 5 min (Fig. S9C). Ablation of RTN3 almost completely blocked CD147 at the PM at all time points analyzed, while clathrin KD had no effect (Fig. S9C). A time-resolved EM analysis showed a progressive reduction of CD147 at the PM, concomitant with its recruitment to TIs, followed by its accumulation in early endosomes (EEs) and, later, in multivesicular bodies (MVBs, Fig. 5E), arguing for CD147 endocytic progression. RTN3 KD strongly affected CD147 accumulation in the different compartments, while leaving unaltered its PM localization (Fig. 5E).

Finally, we analyzed the proximity between CD147-containing NCE structures and the ER. We observed a significant increase in ER-PM contacts upon 2 and 5 minutes of EGF stimulation at CD147-internalizing sites (Fig. 5F and S9D), as also shown by 3D reconstruction of a CD147-positive TI (Fig. 5G and S9E, Movie S1). This phenotype was abolished by RTN3 KD (Fig. 5F), but not by RTN4 KD (Fig. S9F) that had no effect on CD147 internalization (Fig. S9G).

Three other human epithelial cell lines, HaCaT (skin keratinocytes), BT20 (breast cancer) and A431 (skin squamous carcinoma), activated the EGFR/CD147-NCE pathway at high EGF doses in a RTN3-dependent manner (Table S2).

ER contact sites are involved in local Ca^{2+} release required for NCE progression

ER contact sites have a fundamental role in localized Ca^{2+} release (23), which might be relevant to EGFR-NCE. To investigate this, we exploited the Ca^{2+} sensor aequorin, either in a cytoplasmic version (cyto-Aeq) or targeted to the inner leaflet of the PM (PM-Aeq, Fig. S10A); both forms display the same affinity for Ca^{2+} (24). We found that: i) PM-Aeq detected a peak of Ca^{2+} release induced by high, but not low, EGF doses (Fig. 6A and S10B), ii) the Ca^{2+} peak was higher when detected with PM-Aeq *vs.* cyto-Aeq (Fig. 6A), suggesting that it mainly occurs in proximity to the PM, iii) the Ca^{2+} flux did not come from the extracellular space, shown by using the Ca^{2+}-chelator EGTA, which did not affect peak intensity (Fig. S10C), iv) RTN3, but not RTN4, KD strongly impaired the EGF-induced Ca^{2+} response (Fig. 6B and S10D).

These results are compatible with the possibility that Ca^{2+} is released at the PM from the ER, through the formation of EGF-induced RTN3-dependent contact sites. This might occur through the activation of the inositol triphosphate (IP3) receptor (IP3R), which is the main pathway promoting Ca^{2+} release from the ER in HeLa cells (25). Indeed, IP3R inhibition by

xestospongin C strongly affected EGF-induced Ca^{2+} flux at the PM, comparable to RTN3 KD (Fig. 6C), without impairing ER-PM contact site formation at areas of NCE, arguing that Ca^{2+} release is downstream of RTN3-dependent contact site formation (Fig. 6D). IP3R inhibition did not affect NCE-TI formation (Fig. 6E), but it prevented progression of NCE internalization (Fig. 6F,G and S10E) by blocking the fission of TIs (xestospongin C treatment phenocopies dynamin KD causing TI elongation, Fig. 6H and 3C), while having limited impact on CME of EGFR and TfR (Fig. S10E, F).

Discussion

We report here the molecular characterization of EGFR-NCE. We found that proteins previously not suspected to participate in endocytosis are required, among which the ER-resident protein RTN3. We show that at least another cargo, CD147, is trafficked through the same route.

The pathway relies on the establishment of specific RTN3-dependent ER-PM contact sites. A relevant question concerns the mechanistic role of RTN3 in EGFR-NCE. One possibility is that RTN3 might act as a tethering factor between the ER and PM, in regions where EGFR signaling occurs. In favour of this, we showed close proximity between RTN3 and activated EGFR, and specific FRET between the RTN3-EGFR pair at the PM. Importantly, RTN3-dependent contacts involved in EGFR-NCE do not show physical or functional overlap with STIM1- or E-Syt1-dependent contact sites, in agreement with the current idea of contact site specificity (17).

Another possibility is that RTN3 acts in NCE through its “canonical” ER tubulation function. The strongest evidence in this direction is that RTN3 is required for the formation of cortical ER tubules induced by EGF. If this were the case, our data suggest that there must be specificity embedded in the system, since RTN4 KD did not phenocopy the RTN3 KD. In such a scenario, EGFR-emanating signals - whose nature remains to be determined - might exist, which induce ER tubulation at specific sites and by dedicated factors.

RTN3-dependent ER-PM contacts are critical for TI formation. In this context, ER-PM contact sites may serve as an anchor to provide the pulling force required for TI elongation. In addition, these contacts might be involved in one of the emerging functions of ER-biomembrane contacts, which include phosphoinositide and Ca^{2+} signaling, lipid or protein translocation, or in trans regulation of protein function (23). We characterized one such function by establishing that RTN3-mediated ER contacts are involved in EGF-induced local Ca^{2+} release from the ER (IP3R-mediated) to the PM, which occurs only at high EGF dose and is in turn required to finalize the last step of EGFR-NCE, i.e. the fission of TIs. Thus, there is stepwise requirement of RTN3-dependent contact sites in EGFR-NCE (Fig. 6I): i) TI formation/maturation, ii) Ca^{2+} release at ER-PM interface, which is in turn required for, iii) the fission of TIs and the completion of the internalization step. Our data provide evidence for a positive feedback loop between EGFR-NCE and Ca^{2+} signaling: NCE regulates local Ca^{2+} release at ER-PM contact sites, and, in turn, Ca^{2+} flux is required to finalize EGFR-NCE. Interestingly, ER-endosome contact sites have been shown to regulate EGFR signaling

and trafficking also at a later step, in late endosomes/MVBs, and to be modulated by calcium signaling, albeit through a different mechanism (26–28).

In conclusion, we have uncovered a modality of internalization that probably integrates numerous cellular functions towards its execution. NCE has a major role in the regulation of EGFR fate by determining its long-term attenuation. Possible alterations of NCE players can be envisioned to occur in pathological conditions involving aberrant EGFR signaling, first and foremost cancer.

Supplementary Material

Refer to Web version on PubMed Central for supplementary material.

Acknowledgments

We thank P. De Camilli for suggestions and reagents (cDNA of HRP-KDEL and E-Syt1-GFP), G. Scita for suggestions, T. Kirchhausen for TfR cDNA, N. Borgese for Cerulean-17, M. Tagaya for initially providing an anti-RTN3 antibody, R. Lundmark for anti-GRAF1 antibody, D. Cairns for initial statistical analysis of SILAC, the Imaging facility at IFOM, ALEMBIC facility at San Raffaele Institute. We thank R. Gunby and W. Maruwge for critically reading the manuscript. This work was supported by grants from the Associazione Italiana per la Ricerca sul Cancro to TB (IG15741), PP (IG 1442), SP (IG 15637) and PPDF (IG 10349 and 14404 and MCO 10.000); MIUR (the Italian Ministry of University and Scientific Research), the Italian Ministry of Health, and The Monzino Foundation to PPDF; Worldwide Cancer Research to SS (16-1245). ACo is supported by a fellowship from the Fondazione Italiana Ricerca sul Cancro. The authors declare no competing financial interests. All data described in the paper are available in the main text and supplementary materials.

References and Notes

1. Kirchhausen T, Owen D, Harrison SC. Molecular structure, function, and dynamics of clathrin-mediated membrane traffic. Cold Spring Harbor perspectives in biology. May.2014 6:a016725. [PubMed: 24789820]
2. Johannes L, Parton RG, Bassereau P, Mayor S. Building endocytic pits without clathrin. Nat Rev Mol Cell Biol. May.2015 16:311. [PubMed: 25857812]
3. Boucrot E, et al. Endophilin marks and controls a clathrin-independent endocytic pathway. Nature. Jan 22.2015 517:460. [PubMed: 25517094]
4. Sigismund S, et al. Clathrin-independent endocytosis of ubiquitinated cargos. Proceedings of the National Academy of Sciences of the United States of America. Feb 22.2005 102:2760. [PubMed: 15701692]
5. Lund KA, Opresko LK, Starbuck C, Walsh BJ, Wiley HS. Quantitative analysis of the endocytic system involved in hormone-induced receptor internalization. J Biol Chem. Sep 15.1990 265:15713. [PubMed: 1975591]
6. Orth JD, Krueger EW, Weller SG, McNiven MA. A novel endocytic mechanism of epidermal growth factor receptor sequestration and internalization. Cancer Res. Apr 1.2006 66:3603. [PubMed: 16585185]
7. Sigismund S, et al. Clathrin-mediated internalization is essential for sustained EGFR signaling but dispensable for degradation. Developmental cell. Aug.2008 15:209. [PubMed: 18694561]
8. Sigismund S, et al. Threshold-controlled ubiquitination of the EGFR directs receptor fate. Embo J. Jul 31.2013 32:2140. [PubMed: 23799367]
9. Pines G, Kostler WJ, Yarden Y. Oncogenic mutant forms of EGFR: lessons in signal transduction and targets for cancer therapy. FEBS letters. Jun 18.2010 584:2699. [PubMed: 20388509]
10. Ong SE, et al. Stable isotope labeling by amino acids in cell culture, SILAC, as a simple and accurate approach to expression proteomics. Molecular & cellular proteomics : MCP. May.2002 1:376. [PubMed: 12118079]

11. Voeltz GK, Prinz WA, Shibata Y, Rist JM, Rapoport TA. A class of membrane proteins shaping the tubular endoplasmic reticulum. Cell. Feb 10.2006 124:573. [PubMed: 16469703]
12. Shibata Y, et al. The reticulon and DP1/Yop1p proteins form immobile oligomers in the tubular endoplasmic reticulum. The Journal of biological chemistry. Jul 4.2008 283:18892. [PubMed: 18442980]
13. Kirkham M, et al. Ultrastructural identification of uncoated caveolin-independent early endocytic vehicles. J Cell Biol. Jan 31.2005 168:465. [PubMed: 15668297]
14. Sabharanjak S, Sharma P, Parton RG, Mayor S. GPI-anchored proteins are delivered to recycling endosomes via a distinct cdc42-regulated, clathrin-independent pinocytic pathway. Developmental cell. Apr.2002 2:411. [PubMed: 11970892]
15. Lundmark R, et al. The GTPase-activating protein GRAF1 regulates the CLIC/GEEC endocytic pathway. Current biology : CB. Nov 25.2008 18:1802. [PubMed: 19036340]
16. Ferguson SM, et al. Coordinated actions of actin and BAR proteins upstream of dynamin at endocytic clathrin-coated pits. Developmental cell. Dec.2009 17:811. [PubMed: 20059951]
17. Giordano F, et al. PI(4,5)P(2)-dependent and Ca(2+)-regulated ER-PM interactions mediated by the extended synaptotagmins. Cell. Jun 20.2013 153:1494. [PubMed: 23791178]
18. Carrasco S, Meyer T. STIM proteins and the endoplasmic reticulum-plasma membrane junctions. Annual review of biochemistry. 2011; 80:973.
19. Schikorski T, Young SM Jr, Hu Y. Horseradish peroxidase cDNA as a marker for electron microscopy in neurons. Journal of neuroscience methods. Sep 30.2007 165:210. [PubMed: 17631969]
20. Jozsef L, et al. Reticulon 4 is necessary for endoplasmic reticulum tubulation, STIM1-Orai1 coupling, and store-operated calcium entry. The Journal of biological chemistry. Mar 28.2014 289:9380. [PubMed: 24558039]
21. Shi Q, et al. Impact of RTN3 deficiency on expression of BACE1 and amyloid deposition. The Journal of neuroscience : the official journal of the Society for Neuroscience. Oct 15.2014 34:13954. [PubMed: 25319692]
22. Eyster CA, et al. Discovery of new cargo proteins that enter cells through clathrin-independent endocytosis. Traffic. May.2009 10:590. [PubMed: 19302270]
23. Phillips MJ, Voeltz GK. Structure and function of ER membrane contact sites with other organelles. Nat Rev Mol Cell Biol. Feb.2016 17:69. [PubMed: 26627931]
24. Marsault R, Murgia M, Pozzan T, Rizzuto R. Domains of high Ca2+ beneath the plasma membrane of living A7r5 cells. Embo J. Apr 1.1997 16:1575. [PubMed: 9130702]
25. Bennett DL, et al. Expression and function of ryanodine receptors in nonexcitable cells. The Journal of biological chemistry. Mar 15.1996 271:6356. [PubMed: 8626432]
26. Eden ER, White IJ, Tsapara A, Futter CE. Membrane contacts between endosomes and ER provide sites for PTP1B-epidermal growth factor receptor interaction. Nature cell biology. Mar.2010 12:267. [PubMed: 20118922]
27. Haj FG, Verveer PJ, Squire A, Neel BG, Bastiaens PI. Imaging sites of receptor dephosphorylation by PTP1B on the surface of the endoplasmic reticulum. Science. Mar 01.2002 295:1708. [PubMed: 11872838]
28. Kilpatrick BS, et al. An Endosomal NAADP-Sensitive Two-Pore Ca2+ Channel Regulates ER-Endosome Membrane Contact Sites to Control Growth Factor Signaling. Cell Rep. Feb 14.2017 18:1636. [PubMed: 28199837]
29. Sengupta P, et al. Probing protein heterogeneity in the plasma membrane using PALM and pair correlation analysis. Nature methods. Nov.2011 8:969. [PubMed: 21926998]
30. Aboud-Pirak E, et al. Efficacy of antibodies to epidermal growth factor receptor against KB carcinoma in vitro and in nude mice. J Natl Cancer Inst. Dec 21.1988 80:1605. [PubMed: 3193478]
31. Shin KJ, et al. A single lentiviral vector platform for microRNA-based conditional RNA interference and coordinated transgene expression. Proceedings of the National Academy of Sciences of the United States of America. Sep 12.2006 103:13759. [PubMed: 16945906]

32. Uphoff CC, Drexler HG. Comparative PCR analysis for detection of mycoplasma infections in continuous cell lines. In vitro cellular & developmental biology. Animal. Feb.2002 38:79. [PubMed: 11928999]
33. Peters PJ, et al. Characterization of coated vesicles that participate in endocytic recycling. Traffic. Dec.2001 2:885. [PubMed: 11737826]
34. Rappsilber J, Mann M, Ishihama Y. Protocol for micro-purification, enrichment, pre-fractionation and storage of peptides for proteomics using StageTips. Nature protocols. 2007; 2:1896. [PubMed: 17703201]
35. Cox J, Mann M. MaxQuant enables high peptide identification rates, individualized p.p.b.-range mass accuracies and proteome-wide protein quantification. Nature biotechnology. Dec.2008 26:1367.
36. Perkins DN, Pappin DJ, Creasy DM, Cottrell JS. Probability-based protein identification by searching sequence databases using mass spectrometry data. Electrophoresis. Dec.1999 20:3551. [PubMed: 10612281]
37. Nesvizhskii AI. Protein identification by tandem mass spectrometry and sequence database searching. Methods in molecular biology. 2007; 367:87. [PubMed: 17185772]
38. Nesvizhskii AI, Vitek O, Aebersold R. Analysis and validation of proteomic data generated by tandem mass spectrometry. Nature methods. Oct.2007 4:787. [PubMed: 17901868]
39. Penengo L, et al. Crystal structure of the ubiquitin binding domains of rabex-5 reveals two modes of interaction with ubiquitin. Cell. Mar 24.2006 124:1183. [PubMed: 16499958]
40. Schindelin J, et al. Fiji: an open-source platform for biological-image analysis. Nature methods. Jun 28.2012 9:676. [PubMed: 22743772]
41. Schindelin J, Rueden CT, Hiner MC, Eliceiri KW. The ImageJ ecosystem: An open platform for biomedical image analysis. Molecular reproduction and development. Jul-Aug;2015 82:518. [PubMed: 26153368]
42. Meijering EF. J., An ImageJ Plugin Suite for Image Feature Extraction.
43. Heilemann M, et al. Subdiffraction-resolution fluorescence imaging with conventional fluorescent probes. Angewandte Chemie. 2008; 47:6172. [PubMed: 18646237]
44. Thompson RE, Larson DR, Webb WW. Precise nanometer localization analysis for individual fluorescent probes. Biophysical journal. May.2002 82:2775. [PubMed: 11964263]
45. Dempsey GT, Vaughan JC, Chen KH, Bates M, Zhuang X. Evaluation of fluorophores for optimal performance in localization-based super-resolution imaging. Nature methods. Dec.2011 8:1027. [PubMed: 22056676]
46. Wouters FS, Verveer PJ, Bastiaens PI. Imaging biochemistry inside cells. Trends in cell biology. May.2001 11:203. [PubMed: 11316609]
47. Slot JW, Geuze HJ. Cryosectioning and immunolabeling. Nature protocols. 2007; 2:2480. [PubMed: 17947990]
48. Puhka M, Joensuu M, Vihinen H, Belevich I, Jokitalo E. Progressive sheet-to-tubule transformation is a general mechanism for endoplasmic reticulum partitioning in dividing mammalian cells. Molecular biology of the cell. Jul.2012 23:2424. [PubMed: 22573885]
49. Bonora M, et al. Subcellular calcium measurements in mammalian cells using jellyfish photoprotein aequorin-based probes. Nature protocols. Nov.2013 8:2105. [PubMed: 24113784]
50. Pinton P, Pozzan T, Rizzuto R. The Golgi apparatus is an inositol 1,4,5-trisphosphate-sensitive Ca2+ store, with functional properties distinct from those of the endoplasmic reticulum. Embo J. Sep 15.1998 17:5298. [PubMed: 9736609]
51. Renard HF, et al. Endophilin-A2 functions in membrane scission in clathrin-independent endocytosis. Nature. Jan 22.2015 517:493. [PubMed: 25517096]
52. Lakshminarayan R, et al. Galectin-3 drives glycosphingolipid-dependent biogenesis of clathrin-independent carriers. Nature cell biology. Jun.2014 16:595. [PubMed: 24837829]
53. Parton RG, del Pozo MA. Caveolae as plasma membrane sensors, protectors and organizers. Nat Rev Mol Cell Biol. Feb.2013 14:98. [PubMed: 23340574]
54. Swanson JA. Shaping cups into phagosomes and macropinosomes. Nat Rev Mol Cell Biol. Aug. 2008 9:639. [PubMed: 18612320]

55. Frittoli E, et al. The primate-specific protein TBC1D3 is required for optimal macropinocytosis in a novel ARF6-dependent pathway. Molecular biology of the cell. Apr.2008 19:1304. [PubMed: 18199687]

56. Garrett WS, et al. Developmental control of endocytosis in dendritic cells by Cdc42. Cell. Aug 4.2000 102:325. [PubMed: 10975523]

57. Schafer DA, D'Souza-Schorey C, Cooper JA. Actin assembly at membranes controlled by ARF6. Traffic. Nov.2000 1:892. [PubMed: 11273133]

58. Lamaze C, et al. Interleukin 2 receptors and detergent-resistant membrane domains define a clathrin-independent endocytic pathway. Molecular cell. Mar.2001 7:661. [PubMed: 11463390]

59. Grassart A, Dujeancourt A, Lazarow PB, Dautry-Varsat A, Sauvonnet N. Clathrin-independent endocytosis used by the IL-2 receptor is regulated by Rac1, Pak1 and Pak2. EMBO reports. Apr. 2008 9:356. [PubMed: 18344974]

60. Naslavsky N, Weigert R, Donaldson JG. Characterization of a nonclathrin endocytic pathway: membrane cargo and lipid requirements. Molecular biology of the cell. Aug.2004 15:3542. [PubMed: 15146059]

Europe PMC Funders Author Manuscripts

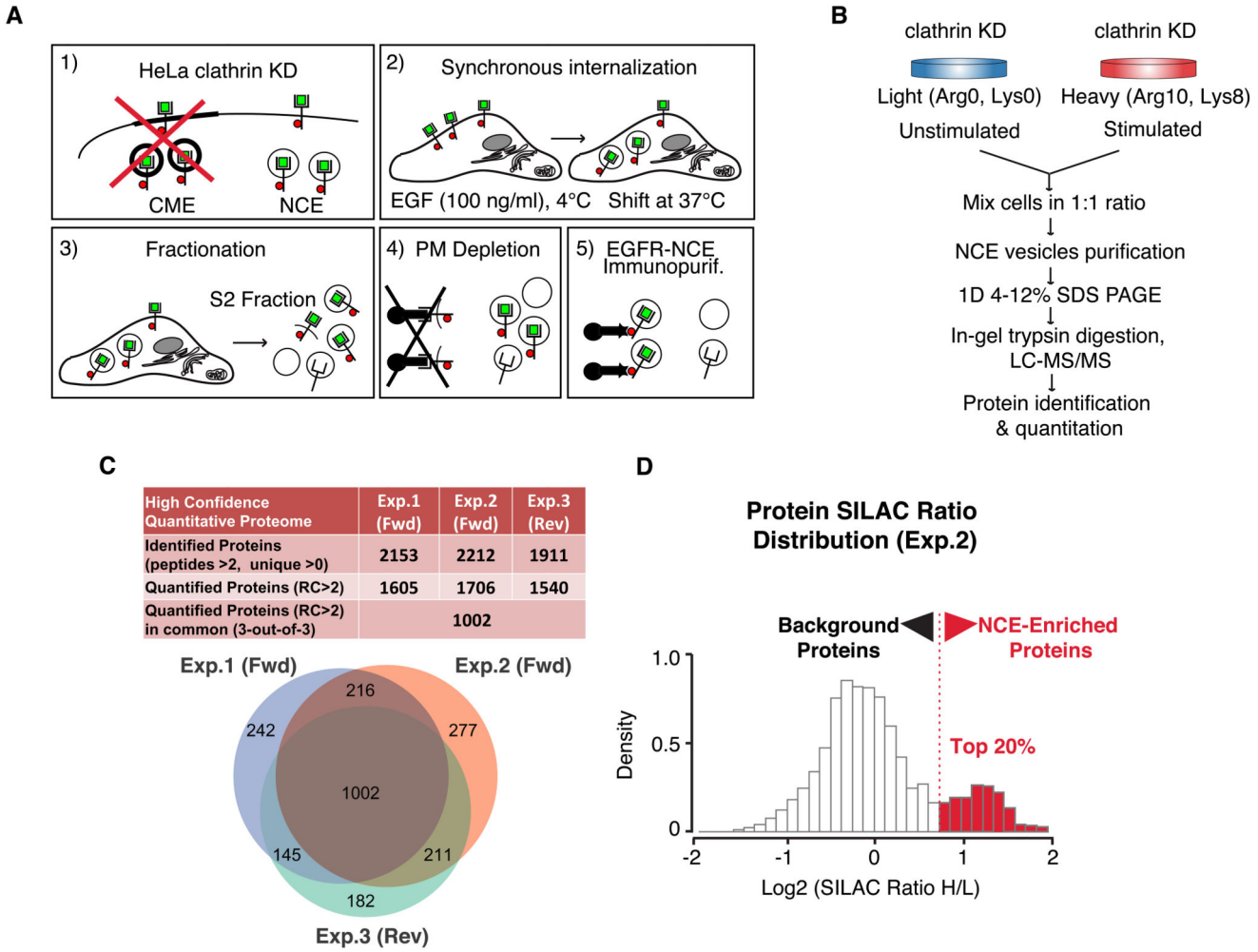

High Confidence Quantitative Proteome	Exp.1 (Fwd)	Exp.2 (Fwd)	Exp.3 (Rev)
Identified Proteins (peptides >2, unique >0)	2153	2212	1911
Quantified Proteins (RC>2)	1605	1706	1540
Quantified Proteins (RC>2) in common (3-out-of-3)	1002		

Figure 1. Molecular components of EGFR-NCE.

(**A**) Purification of NCE vesicles. HeLa clathrin KD cells (1) were subjected to a synchronous wave of EGFR internalization (2), and then to subcellular fractionation (3), to obtain the S2 fraction. The S2 fraction was subjected to a PM depletion step with anti-EGFR (against the extracellular domain) (4), and to immunopurification with anti-phosphoEGFR (5). (**B**) SILAC-MS analysis; EGF stimulation and vesicle purification were as in (A). (**C**) Numbers of quantified proteins in three SILAC experiments (2 forward, Fwd; 1 reverse, Rev). Venn diagram: overlap among the identified proteins. (**D**) SILAC H/L ratios distribution of all proteins confidently quantified (RC>2) in Exp. 2 (other experiments are in File S1, spread-sheet 2). The enriched proteins (top 20%) are in red.

A

Gene	Localization/ function	EGFR Ke reduction (%) in high EGF: Gene KD	Gene KD + clath. KD
RTN3	ER membrane	42	68
REEP5	ER membrane	33	68
P4HB	ER enzyme	28	69
PLOD1	ER enzyme	50	71
ECHS1	Mito. enzyme	16	72
LRPPRC	Mito/RNA bind.	24	71
KHDRBS1	RNA bind/signaling	16	65
ZFR	RNA bind/Zn finger	22	70
TPR	nuclear export	15	68
dynamin	CME + NCE	80	80
clathrin	CME	50	-

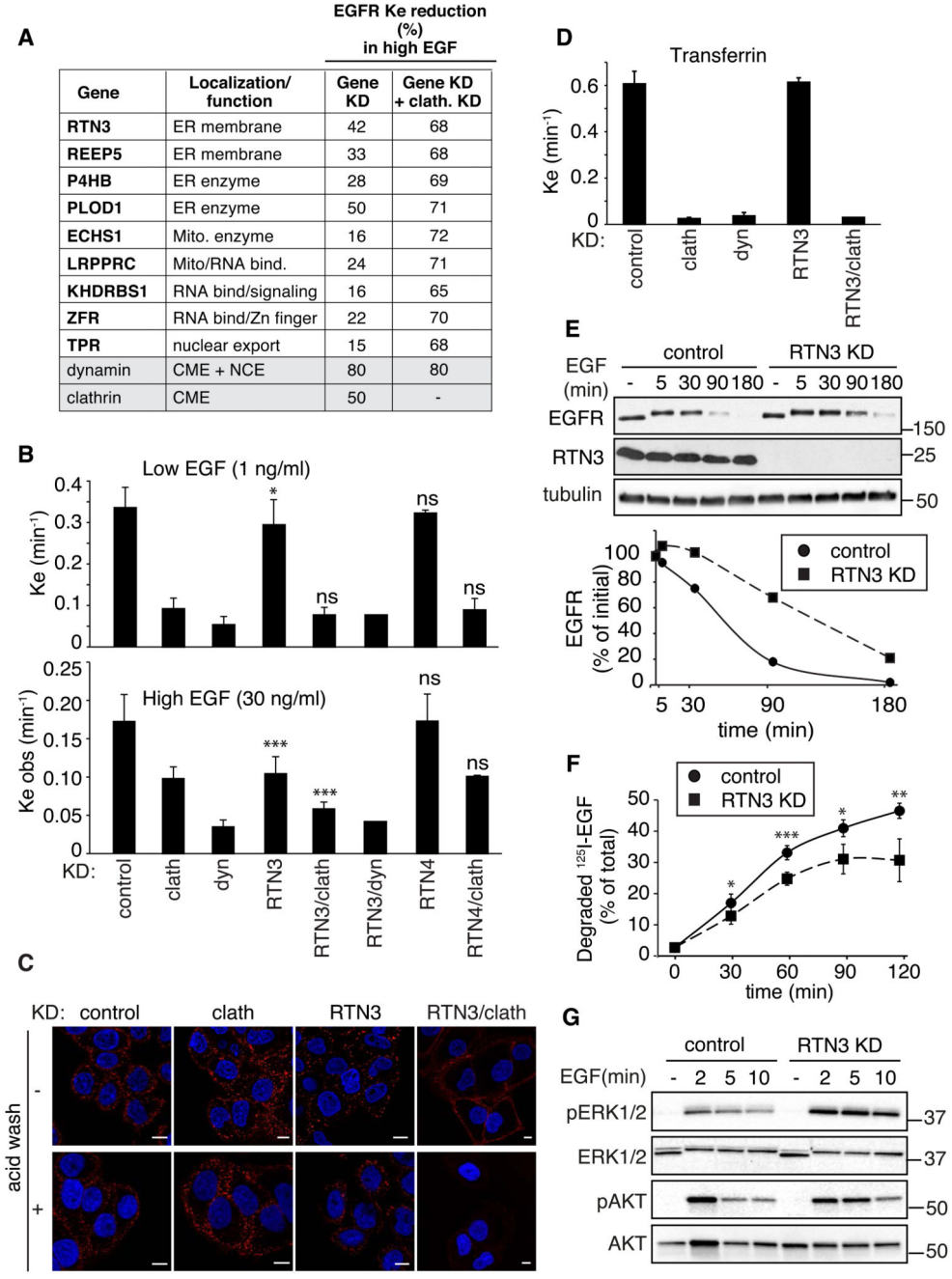

Figure 2. RTN3 and EGFR-NCE.

(**A**) EGFR-NCE regulators are shown. EGFR internalization is expressed as the reduction in the Ke *vs.* control (measured at high EGF, by ^{125}I-EGF internalization assays). Clathrin and dynamin, controls. (**B**) Internalization constants at low and high EGF doses upon the indicated KDs. Here and in the other panels, data are the mean ± SD and P-values were calculated using Each Pair Student's t test. P-values are for RTN3 or RTN4 *vs.* control; RTN3/clath or RTN4/clath *vs.* clath; ***, P <0.001; *, <0.05; ns, non-significant. (**C**) Internalization of Alexa555-EGF (red) 8 min after stimulation, in the indicated conditions.

Bar, 10 μm. Blue, DAPI. (**D**) Ke of ^{125}I-Tf internalization in the indicated conditions. Data are the mean ± SD. (**E**) Top, EGFR degradation (EGF, 100 ng/ml). Bottom, densitometric quantification, expressed as the percentage of EGFR levels relative to the initial amount. (**F**) Quantitative ^{125}I-EGF degradation assay. Data are expressed as percentage of degraded EGF. *, P <0.05, **, <0.01, ***, <0.001 (*vs.* control). (**G**) Analysis of EGF-dependent signaling in the indicated conditions (EGF, 100 ng/ml).

Europe PMC Funders Author Manuscripts

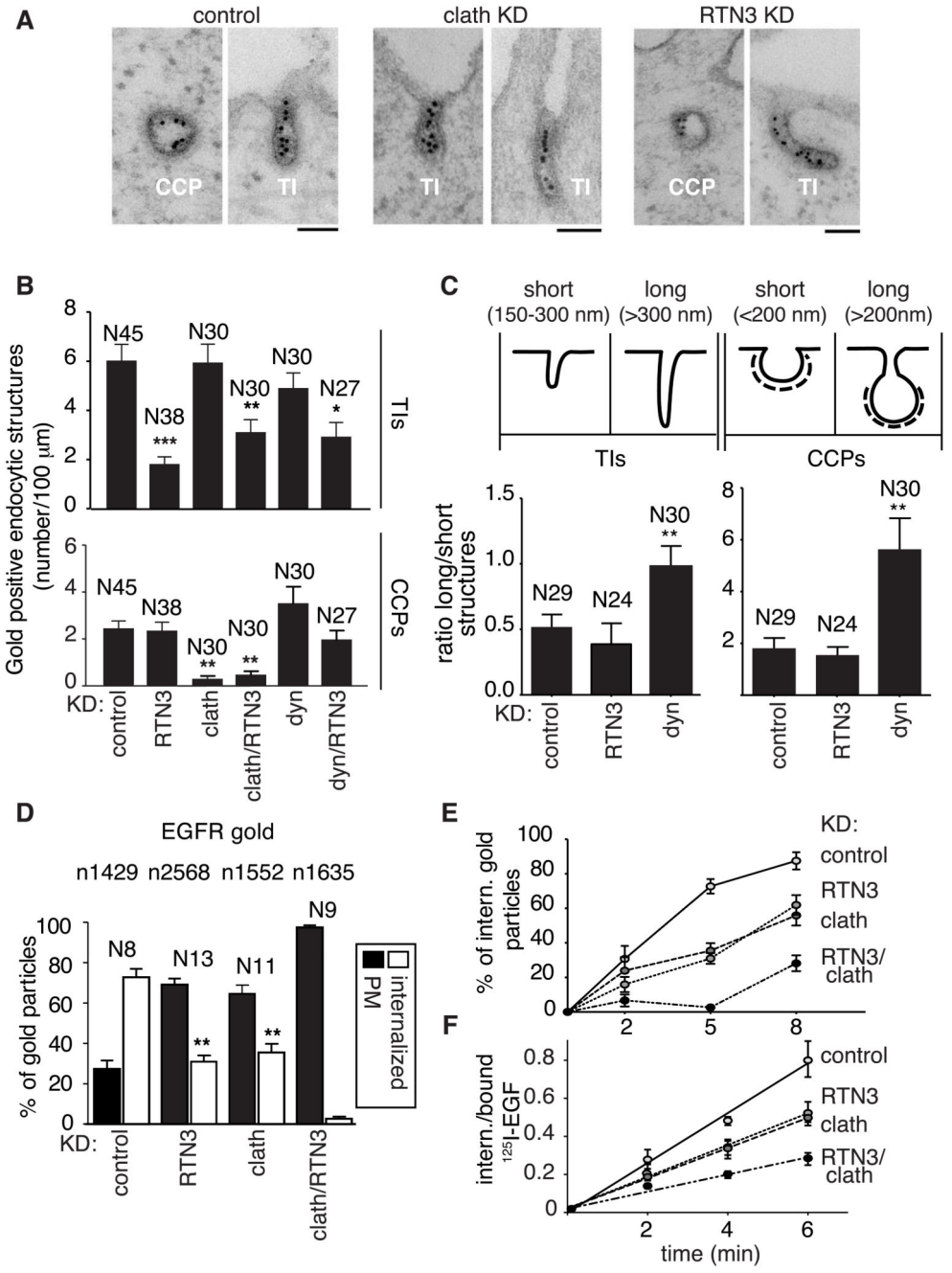

Figure 3. Characterization of EGFR-NCE by EM.

(**A**) Representative EGFR endocytic structures, upon high EGF. Bar 100 nm. (**B**) Quantitation of gold-EGFR positive TIs and CCPs (5 minutes of high EGF). Only RuR-stained structures were counted. N, cell profiles analyzed. Data are expressed as the number of gold-positive structures, normalized to PM profiles of 100 µm length, ± SEM. Here and in the other panels, P-values were calculated using One-way ANOVA. *, P <.05, **, <0.01, ***, <0.001 (*vs.* control). (**C**) Morphometric analysis of the length of EGFR gold-positive TIs and CCPs (top). Data (bottom) are expressed as the ratio between the number of long/

short structures normalized to PM profiles of 100 μm length ± SEM. N, cell profiles analyzed. *, P <.05, **, <0.01 (*vs.* control). (**D**) Quantitation of PM *vs.* internalized EGFR (gold-labeled) upon high dose EGF (5 min). Data are the mean ± SEM. N and n, cell profiles and gold particles, respectively. ***, P <.001, RTN3 KD or clath KD *vs.* control, RTN3+clath KD *vs.* clath KD (or RTN3 KD). (**E**) Percentage of internalized gold particles as a function of time of EGF stimulation. (**F**) ^{125}I-EGF internalization kinetics at high dose EGF.

Europe PMC Funders Author Manuscripts

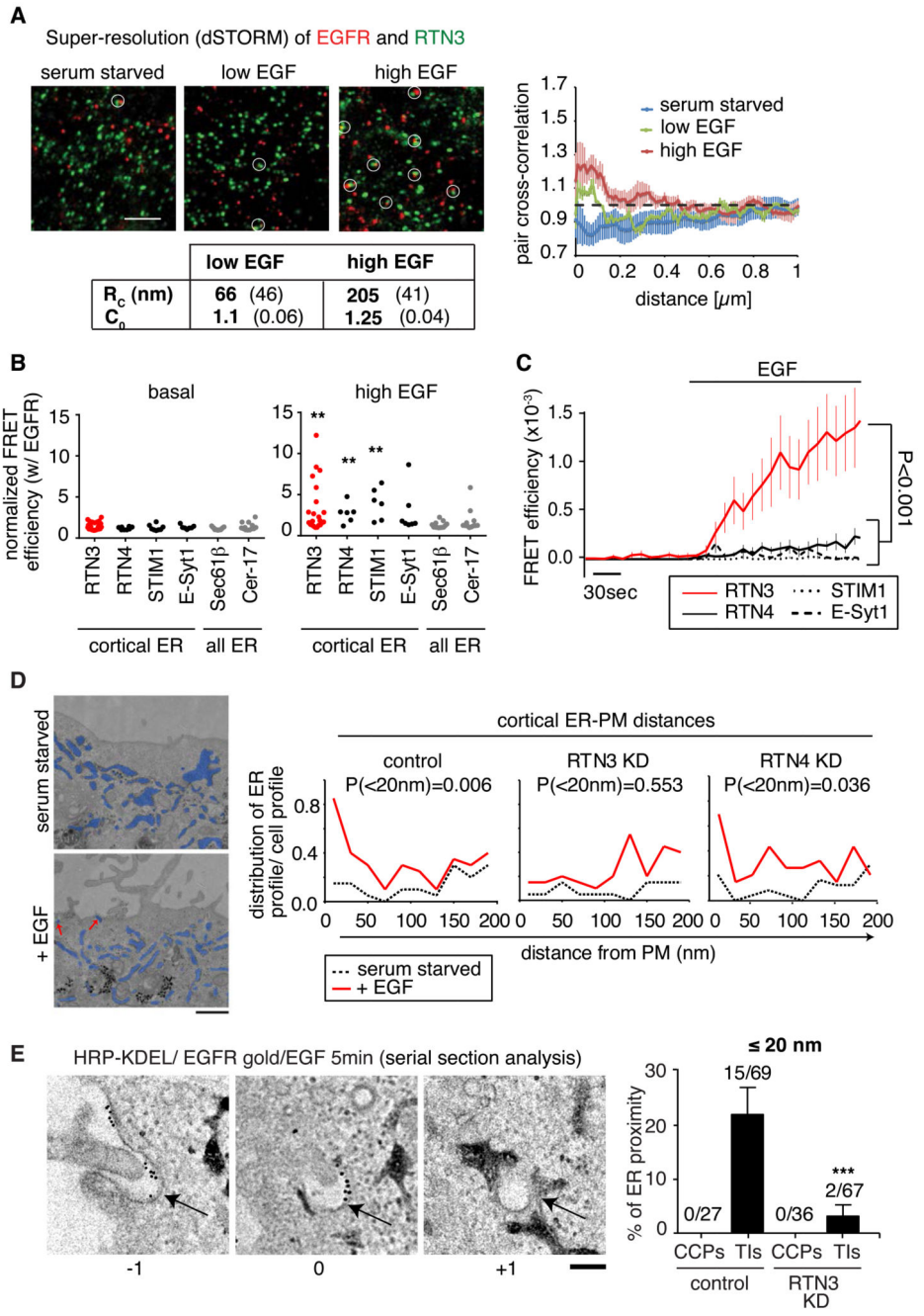

Figure 4. RTN3-mediated contacts at site of EGFR-NCE.

(**A**) dSTORM of RTN3 (green) and EGFR (red). Left, images of cells in the indicated conditions. Bar, 0.7 μm. Right, cross-correlation between the two channels as a function of distance (29). Bottom left, C_0, amplitude of the correlation, proportional to the fraction of co-clustered RTN3/EGFR signals, and R_C, spatial extent of the cross-correlation curve, which is an estimate of co-cluster size. 95% confidence intervals (CI) are in parenthesis. (**B**) Sensitized Emission FRET analysis (SE-FRET). Shown are the normalized SE-FRET efficiencies of EGFR-EYFP with the indicated ECFP-tagged constructs or cerulean-17

Europe PMC Funders Author Manuscripts

(Cer-17), before (basal, left) and after 5 min stimulation with high dose of Alexa555-EGF (high EGF, right). RTN3 (red), cortical ER-enriched proteins (“cortical ER”, black), non-cortical-enriched ER proteins (“all ER”, grey). P-values were calculated by Two Tailed Student’s t test. **, P <0.01 (EGF-stimulated *vs.* basal condition). (**C**) Proximity measurement at the PM. SE-FRET as in (B) was restricted to PM regions where EGFR is activated, and to 3 min of EGF stimulation. P-values were calculated by One-way ANOVA. (**D**) Left, representative EM images showing distribution of juxta-PM ER profiles. Blue, general ER profiles; arrows indicate ER profiles <20 nm from the PM. Bar, 1 μm. Right, number of ER profiles at various distances from the PM in 20 random images/condition ± EGF stimulation. P-value for EGF-stimulated *vs.* unstimulated cells (Mann-Whitney Test). (**E**) Left, representative serial sections showing contacts (≤20 nm) between ER and gold-EGFR-positive structures. Arrows indicate the same structure across sections. Bar, 100 nm. Right, mean frequency of ER proximity with gold EGFR-labeled CCPs or TIs at 5 min of EGF stimulation, expressed as percentage ± SEM. The number of counted structures in contact with the ER is indicated (distance ≤ 20 nm). P-values were calculated by Two Tailed Student’s t test. ***, P <0.001 (*vs.* control TIs).

Europe PMC Funders Author Manuscripts

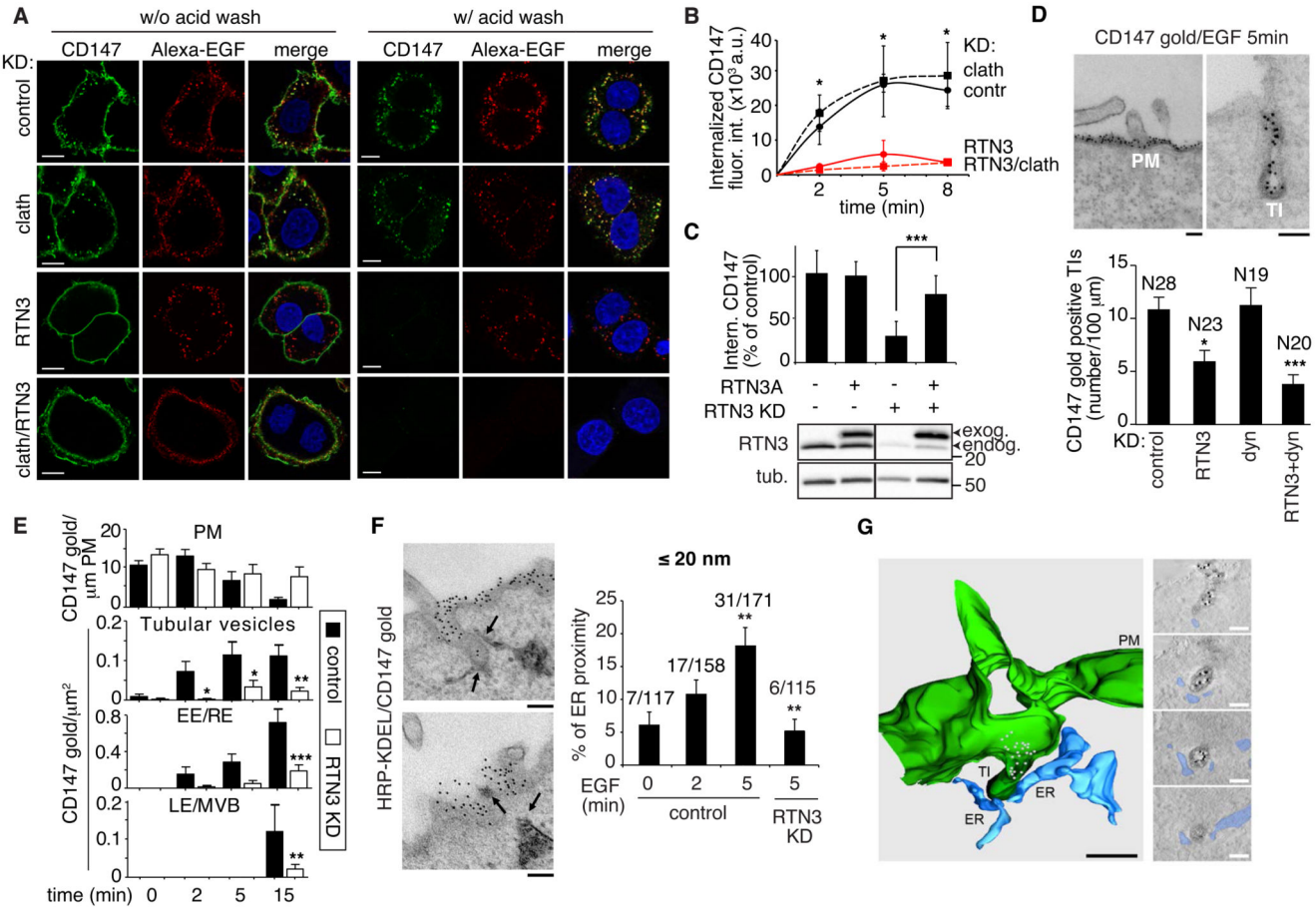

Figure 5. RTN3-dependent CD147 internalization.

(**A**) CD147 (green) internalization at 8 min of Alexa555-EGF. Prior fixation, cells were acid-wash treated (to eliminate PM-EGF/CD147) or untreated. Bars, 10 µm. Blue, DAPI. (**B**) Time course of CD147 internalization after EGF addition. Mean integrated fluorescence intensity ±SD is reported (a.u., arbitrary units). P-values were calculated by Each Pair Student's t test. *, P<0.05 (RTN3 *vs.* control). (**C**) Rescue of CD147 internalization in RTN3 KD cells upon expression of RNAi-resistant RTN3-Isoform A (Fig. S8A,B). Top, quantitation as in panel (B). Integrated fluorescence intensity was reported as % of each control line ± SD. P-values were calculated by Two Tailed Student's t test. ***, P <0.001. Bottom, RTN3 endogenous and exogenous levels (arrows) were analyzed by IB. This panel was assembled from samples run on the same gel by splicing out the irrelevant lanes. (**D**) Top, EM representative images of CD147-positive structures in high EGF-stimulated cells (5 min). Bar, 100 nm. Bottom, quantitation of RuR-stained gold-CD147-positive TIs. N, cell profiles analyzed. Data are expressed as the number of gold-positive structures/PM profiles of 100 µm length ± SEM. P-values were calculated by Two-tailed Student's t test. *, P <0.05; ***, <0.001 (*vs.* control). (**E**) Quantitation of gold-CD147 ± SEM in control and RTN3 KD cells. P-values were calculated by One-way ANOVA. *, P <0.05; **, <0.01; ***, <0.001 (RTN3 KD *vs.* control). (**F**) Left, representative contact sites between ER and gold-CD147-labeled structures. Bar, 100 nm. Right, mean frequency of the proximity between ER

Europe PMC Funders Author Manuscripts

and CD147-positive structures upon high EGF dose. Data are expressed as percentage ± SEM. **, P <0.01 (One-way ANOVA, control 2 min or 5 min *vs.* control 0 min; Two-tailed Student's t test, RTN3 5 min *vs.* control 5 min). (**G**) 3D reconstruction of a CD147-positive (white dots) TI at the PM (green) in contact with the ER (light blue). Bar, 200 nm. Slices of the tomogram are provided on the right (ER pseudocolored in blue). Bar, 100 nm.

Europe PMC Funders Author Manuscripts

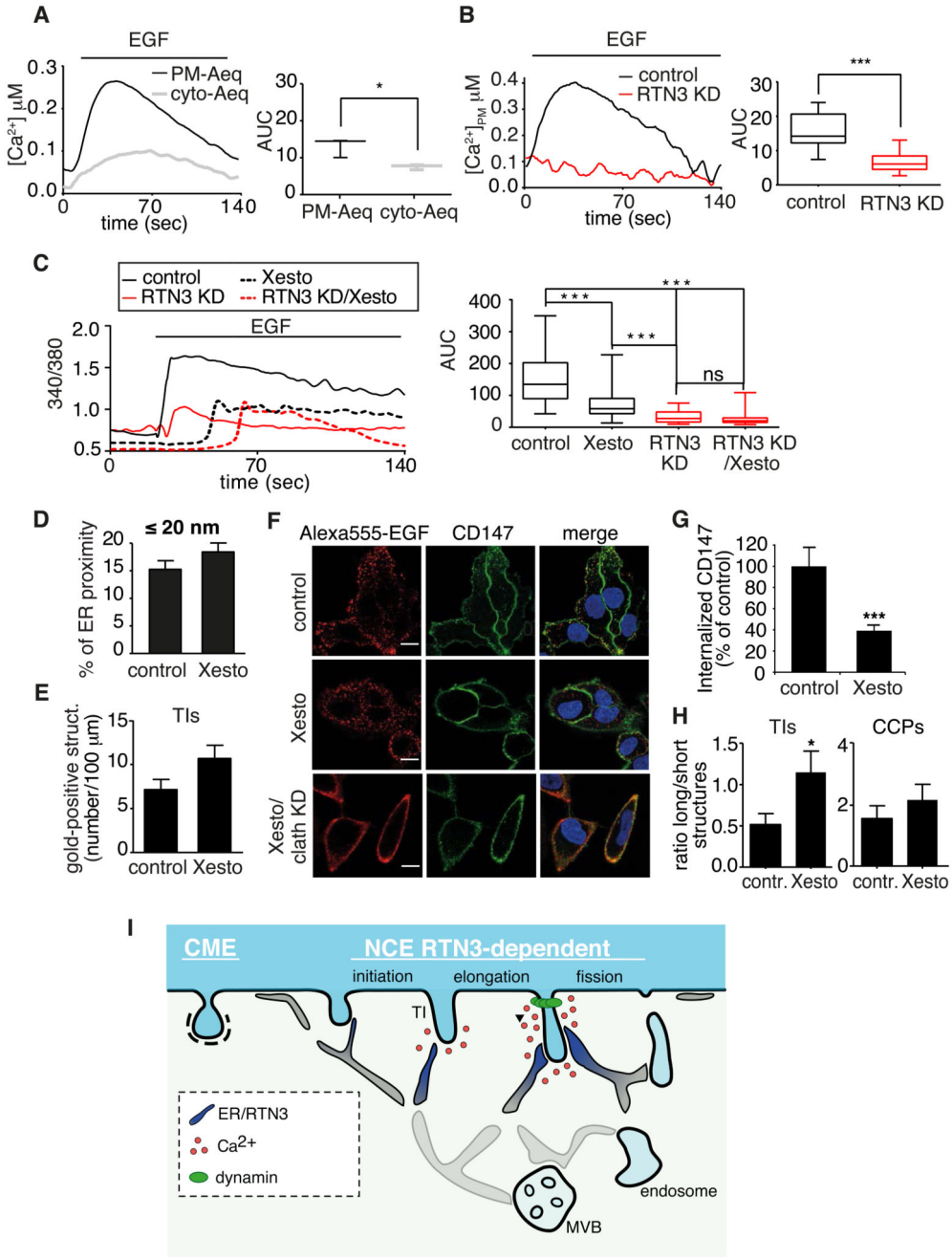

Figure 6. RTN3 is required for EGF-induced Ca^{2+} release at ER-PM contact sites.

(**A**) Left, measurements of $[Ca^{2+}]$ upon high dose EGF (100 ng/ml), with cytosolic aequorin (cyto-Aeq, grey) or PM-targeted aequorin (PM-Aeq, black). Right, area under the curve (AUC). Here and in panel B, P-values were calculated by Two Tailed Student's t test. *, P<0.05. (**B**) Left, measurements of $[Ca^{2+}]_{PM}$ with PM-aeq upon high dose EGF (100 ng/ml). Right, AUC. ***, P<0.001. (**C**) Left, representative cytosolic Ca^{2+} response upon high dose EGF in control and RTN3 KD cells, treated or not with xestospongin C (Xesto) and loaded with Fura-2, AM. Ratio of fluorescence at 340/380 nm is reported. Right, AUC. P-values

were calculated by One-way ANOVA. ***, P<0.001. (**D**) Mean frequency of proximity between ER and CD147-positive structures upon high dose EGF for 5 min. n, number of CD147-positive structures analyzed. Percentage ± SEM is reported. Here and in panels E, G and H, P-values were calculated by Two Tailed Student's t test. (**E**) Quantitation of gold-CD147-positive TIs at 5 min high dose EGF. Only RuR-stained structures were counted. N, number of cell profiles analyzed. Data are expressed as the number of gold-positive structures/PM profiles of 100 μm length ± SEM. (**F**) CD147 (green) internalization after 8 min of Alexa555-EGF (red). Bars, 10 μm. Blue, DAPI. (**G**) Quantitation of CD147 internalization as in Fig. 5B. Integrated fluorescence intensity ± SD. ***, P<0.001. (**H**) Morphometric analysis of EGFR gold-positive TIs (left) and CCPs (right). Data are expressed as the ratio between the number of long/short structures (defined as in Fig. 3C top) normalized to PM profiles of 100 μm length. N, number of cell profiles analyzed. *, P<0.05. (**I**) Model for EGFR endocytosis. At high EGF, EGFR is internalized through CME and NCE. NCE is mediated by PM invaginations that require the formation of RTN3-dependent ER contact sites to progress. Once TIs are formed, contacts sites are needed for local Ca^{2+} release, in turn required for the fission of NCE-TI.

Europe PMC Funders Author Manuscripts